Uptake of chloride and carbonate by Mg-Al and Ca-Al layered double hydroxides in simulated pore solutions of alkali-activated slag cement

Xinyuan Ke[a], Susan A. Bernal[a,b], John L. Provis[a,*]

[a] *Department of Materials Science and Engineering, Sir Robert Hadfield Building, The University of Sheffield, Sheffield S1 3JD, United Kingdom*
[b] *Department of Civil and Structural Engineering, Sir Frederick Mappin Building, The University of Sheffield, Sheffield S1 3JD, United Kingdom*

ARTICLE INFO

ABSTRACT

Chloride ingress and carbonation are major causes of degradation of reinforced concrete. To enable prediction of chloride ingress, and thus to improve the durability of structural alkali-activated slag cement (AAS) based concretes, it is necessary to understand the ionic interactions taking place between chlorides, carbonates, and the individual solid phases which comprise AAS. This study focused on two layered double hydroxides (LDH) representing those typically identified as reaction products in AAS: an Mg-Al hydrotalcite-like phase, and an AFm structure (strätlingite), in simulated AAS pore solutions. Surface adsorption and interlayer ion-exchange of chlorides occurred in both LDH phases; however, chloride uptake in hydrotalcite-group structures is governed by surface adsorption, while strätlingite shows the formation of a hydrocalumite-like phase and ion exchange. For both Ca-Al and Mg-Al LDHs, decreased chloride uptakes were observed from solutions with increased $[CO_3^{2-}]/[OH^-]$ ratios, due to the formation of carbonate-containing hydrotalcite and decomposition of AFm phases, respectively.

1. Introduction

Corrosion of steel reinforcement is one of the main causes of structural failures of reinforced concrete. The combined increase of free chloride ion concentration and decrease of pH in the pore solution (e.g. as a result of carbonation in the binding matrix), particularly at the interface between the steel rebar and the cementitious matrix, are critical conditions leading to initiation of steel corrosion [1–3].

Alkali-activated slag (AAS) cements, produced via a chemical reaction between a granulated blast furnace slag and an alkaline solution [4], often exhibit low chloride permeability compared with Portland cement [5–7]. This has been partially attributed to the reduced capillarity identified in these materials [8,9], and the high concentration of free ions (including Na^+ and OH^-) present in the pore solution may also generate an osmotic gradient to counteract migration of Cl^-. The potentially high chloride binding capacity of the AAS cement binder postulated in some studies might also contribute to the higher resistance to chloride ingress [5,6], and this is the core question to be examined in the current study. The retention of chlorides in the alkali-activation reaction products by chemical binding would be expected to delay the ionic transport of chlorides through the concrete, thus reducing the chloride migration rate [10].

It can be expected that the chloride binding capacity of AAS cements is largely dependent on the chloride binding capacities of the individual phases forming in these systems (e.g. LDHs and (Al,Na)-substituted calcium silicate hydrate (C-(N)-A-S-H) type gels), whose type and relative concentrations are governed by the chemistry of both the slag [11,12] and the alkali-activator [13,14]. However, no evidence has been provided in the literature regarding the influences of the different phases present in AAS cements on chloride binding. Understanding the ionic binding capacity of chlorides of each individual phase forming in cementitious matrices is crucial for determining the rate of chloride transport, and thus for correctly predicting the long term performance of concretes based on these cements [10,15,16].

Layered double hydroxides (LDHs), with a general formula of $[M_{1-x}^{II}M_x^{III}(OH)_2]^{x+}[A^{m-}]_{x/m}\cdot nH_2O$, are a group of minerals that have a positively charged layered structure due to partial substitution of divalent by trivalent cations in a brucite-like lattice structure, yielding a capacity for anion exchange in the interlayer [17–19]. Two types of layered double hydroxides (LDHs) are commonly identified as important reaction products in AAS pastes, as well as in blends of Portland cement with high contents of blast furnace slag: Mg-Al-LDH phases with a hydrotalcite-like structure; and Ca-Al-LDH phases with a hydrocalumite-like structure, also referred to as AFm phases. The physicochemical properties of these phases are subject to the slag chemistry and, in AAS, the type of activator used [4,11–13,20].

Hydrotalcite-like phases are often identified when slags with moderate to high MgO content (> 5 wt%) are used to produce AAS, particularly with sodium silicate, hydroxide or carbonate activators [11–13]. An Mg/Al molar ratio between 2 and 3 generally characterises hydrotalcite-group minerals [21]; Mg/Al ~ 2.1 has been observed in long-term (over 6 months) cured AAS samples using either sodium hydroxide or sodium silicate as activators [11–13,20], and also predicted through thermodynamic modelling [22]. However, higher Mg/Al ratios have also been reported in some sodium silicate activated slag samples, e.g. Mg/Al ~ 2.3 after 1 year of curing [23], and Mg/Al ~ 2.6 after 90 days of curing [24]. The higher Mg/Al ratio of around 2.5 characterised in potassium hydroxide-activated slag samples after 8 years of curing also indicates that the alkali metal present in the activator has a significant influence on the chemistry of the hydrotalcite-like phase formed in AAS cement binders [25]. More ordered hydrotalcite-likes phase are identified in sodium hydroxide-activated and sodium carbonate-activated slag cements, while less structural ordering was identified in sodium silicate-activated slag paste [12,13,26].

AFm-like Ca-Al LDH phases have also been identified in AAS cements, generally with a Ca/Al ratio fixed at 2 but with different interlayer species, including hydroxide, carbonate, sulfate, and aluminosilicate anions [13,20,25,27–29]. In slag cements activated by sodium hydroxide or sodium silicate, the AFm type phase strätlingite, with an aluminosilicate interlayer anion $[AlSi(O_8H_8)\cdot0.25H_2O]^-$, has been identified [20,28]. This mostly appears to be present in AAS in disordered forms that are difficult to detect by X-ray diffraction, which may indicate partial ionic substitution in this interlayer site, but this phase has been predicted from thermodynamic modelling to be very important in the phase assemblages of these binders at later age [22]. Conversely, in sodium carbonate-activated slag cement, the crystalline AFm phase calcium monocarboaluminate was identified as a reaction product in mature samples [13,29], consistent with the thermodynamic modelling predictions reported by Myers et al. [22]. Calcium hemicarboaluminate has also been identified in some early age sodium carbonate-activated slag paste samples [13].

Chloride-bearing equivalents of these two types of LDH phases have been reported in Portland cement based systems, binding chloride from external sources mainly through an ion-exchange mechanism in the interlayer [30–35]. Previous studies [36,37] showed that chloride ions are mostly identified in the diffuse layer at the external surface of hydrotalcite-like phase, pairing with Na^+. The formation of a chloride-exchanged hydrotalcite-like phase has been claimed [38,39], however there is not yet sufficient information to describe its mineralogy. For AFm-phases, although the $AFm(SO_4,Cl)$ [31], $AFm(CO_3,Cl)$ [30,31] and $AFm(OH,Cl)$ [35] solid solutions have been evaluated, the interaction of chloride ions with strätlingite has not yet been characterised in detail.

The interactions controlled by surface adsorption (physical sorption) on the LDH phases studied here have been evaluated in the literature only to a limited degree. Chloride uptake can take place through surface adsorption in the diffuse electrical double layer (EDL) outside the positively charged LDH surface [17,36,40]. Also, given that the surfaces of LDHs are hydroxylated, the pH in the solution may affect the surface adsorption process by influencing the charge density of the surface [36,41]. Florea and Brouwers [42] studied the physical sorption of NaCl onto Friedel's salt in Portland cement based systems, but found no significant effect. However, in AAS cement, the pore solution is of high alkalinity (approximately 1.0 mol/L NaOH [22,43]) and high ionic strength, thus greater surface adsorption on both types of LDH phase is expected.

Atmospheric carbonation of AAS leads to a reduction in alkalinity and an increase in the concentration of dissolved carbonates in the pore solution [44,45]. Carbonate ions may also play important roles in determining chloride uptake by the solid phases present in AAS cement; CO_3^{2-} can be taken up by LDH interlayers to form stable mineral phases [36]. However, there has not been previous investigation of the stability of the chloride-bearing LDHs in presence of carbonate ions, in simulated pore solutions relevant to AAS cements.

In order to create a database which can be used in determining the chloride binding capacity of AAS paste as a whole, this study focuses on determination of the chloride binding capacities of a synthetic hydrotalcite-like phase and strätlingite, in chloride-rich simulated pore solutions with varying $[Cl^-]/[OH^-]$ and $[CO_3^{2-}]/[OH^-]$ ratios. Changes in chemistry and mineralogy in both LDHs were determined using X-ray fluorescence spectrometry (XRF), X-ray diffraction (XRD) and thermogravimetry coupled with mass spectrometry (TG-MS). The respective contributions of surface adsorption and interlayer incorporation have also been determined.

2. Experimental methodology

2.1. Mg-Al hydrotalcite-like phase

A calcined layered double hydroxide (CLDH) was produced from thermally treated synthetic hydrotalcite ($Mg_{0.7}Al_{0.3}(OH)_2(CO_3)_{0.15}\cdot0.63H_2O$, Sigma-Aldrich), following the same method as described in [13], with an Mg/Al ratio of 2.0 to 2.3, and residual carbonate content lower than 0.1 wt%. The CLDH is used for studying the ion-exchange capacity of hydrotalcite-like phases, because as it recrystallises to its layered double hydroxide structure with Mg and Al in the positively charged metal oxide sheet, the anions intercalated into the interlayers are able to be controlled according to the anions present in the aqueous phase [13].

2.2. AFm phase-strätlingite

Strätlingite ($Ca_2Al(AlSi)O_2(OH)_{10}\cdot2.25H_2O$) was prepared according to the method described by Matschei et al. [46]. Initially, stoichiometric quantities of CaO (obtained by calcining $CaCO_3$ (Sigma-Aldrich) at 1000 °C for 12 h), $Na_2SiO_3\cdot9H_2O$ (Sigma-Aldrich, ≥ 98%), and $NaAlO_2$ (Sigma-Aldrich), were separately suspended in Milli-Q water, at 20 ± 3 °C. Then, the sodium aluminate slurry was added to the portlandite suspension formed by hydration of CaO. After shaking for 1 min, the sodium silicate solution was added into the mixture, which was sealed in HDPE bottles with Parafilm. The HDPE bottles were kept at 20 ± 3 °C and agitated daily for 6 weeks. Preparation of the synthetic strätlingite was carried out in a nitrogen filled glove box to minimise any potential for carbonation.

2.3. Ion-exchange in chloride-rich simulated pore solutions

Two groups of chloride rich simulated pore solutions were prepared: carbonate-free solutions and carbonated solutions (compositions shown in Table 1). Four carbonate-free solutions were prepared, with a constant total Na^+ concentration and total ionic strength, but with varying $[Cl^-]/[OH^-]$ ratios. Two carbonated simulated pore solutions

Table 1
Stoichiometric compositions of the simulated chloride-rich pore solutions studied.

	Concentration (mol/L)				$[Cl^-]/$ $[OH^-]$	Total ionic strength, I (mol/L)
	NaCl	NaOH	Na_2CO_3	Total Na^+		
Carbonate-free solutions						
CH-1	0.10	0.90	0	1.00	0.1	1.00
CH-2	0.25	0.75	0	1.00	0.3	1.00
CH-3	0.50	0.50	0	1.00	1.0	1.00
CH-4	0.75	0.25	0	1.00	3.0	1.00
Carbonated solutions						
CH3-1	0.50	0.30	0.10	1.00	1.7	1.10
CH3-2	0.50	0.10	0.10	0.80	5.0	0.90

were designed: solution CH-3-1 has the same total Na^+ concentration as the carbonate-free solutions, but with hydroxides partially replaced by carbonate ions, resembling the natural carbonation process (Eq. (1)) [45]. Solution CH-3-2 was designed for investigating the effect of hydroxide concentration on chloride binding in the presence of carbonate, therefore the chloride concentration and carbonate concentration were matched to CH-3-1, but with a much lower hydroxide concentration.

$$2OH^- + CO_2 \rightarrow H_2O + CO_3^{2-} \tag{1}$$

To study the interaction of chloride-rich simulated pore solution with the synthetic LDHs, 40 g of pre-prepared solutions (Table 1) were weighed in 50 mL centrifuge tubes, and 0.4 g of solids (either CLDH or strätlingite) were added to each, under a nitrogen atmosphere in a glove box. Each formulation was prepared in duplicate. The specific solid to liquid ratio was chosen to ensure that, even at the lowest chloride concentration studied, the total chloride content in the liquid phase would be sufficient to occupy all the available ion-exchangeable interlayer sites. All tubes were sealed with Parafilm to minimise water evaporation and sample carbonation, stored at 20 ± 3 °C, and were manually shaken for 3 min every day until the mixtures reached equilibrium.

2.4. Test methods

After reaching equilibrium (7 days for CLDH [47], and 3 weeks for strätlingite [48]), the LDHs mixed/reacted with the different Cl-rich solutions (Table 1), were separated from the chloride-rich solution using a centrifuge (Heraeus Biofuge Primo) at 4000 min⁻¹ for 6 min. Prior to analysis, the separated supernatant solutions were filtered through 0.45 μm PVDF filter membranes. The pH values of the supernatants were determined using a digital pH meter (Oakton Acorn Series). The chloride ionic concentration was obtained using an ion selective electrode (Cole-Parmer Epoxy solid-state chloride electrode, accuracy ± 2%) according to ASTM D512–12 [49]. The chloride binding capacity of CLDH was calculated using Eq. (2).

$$Q_e = (C_e - C_0) \cdot V / m_{input} \tag{2}$$

Q_e - Chloride binding capacity of solid, mg/g (by dry mass of initial solid).

C_e - Chloride concentration of the supernatant solution, mol/L.

C_0 - Initial chloride concentration, mol/L.

V - Volume of solution, mL.

m_{input} - Initial mass of solid, g.

After chloride immersion, two sets of solid LDH samples were conditioned. The first group of samples were dried in a vacuum desiccator at a controlled relative humidity at 30 ± 3% (reached using saturated $CaCl_2$ salt) for 4 days, immediately after the first filtration. These samples are referred to as "*first filtration samples*" throughout this paper. The second group of LDH samples were washed with Milli-Q water, following the RILEM recommendations for analysis of water soluble chloride content in concrete [50], centrifuged and separated again. The solids were then dried under the same conditions as described for the first filtration samples. These samples are referred to as "*second filtration samples*".

The chemical compositions of the solid LDHs were analysed using a Panalytical Zetium Wavelength dispersive X-ray Fluorescence (XRF) Analyser. A 4 kW rhodium X-ray source was used. Ground solid powder samples were pressed into pellets prior to measurement.

X-ray diffraction (XRD) analysis of LDH solids after the first and the second filtration was carried out using a Bruker D2 Phaser instrument, with Cu Kα radiation and a nickel filter. The tests were conducted with a step size of 0.02° and a counting time of 0.5 s/step, from 5° to 70° 2θ for the hydrotalcite-like phase, and from 5° to 50° 2θ for strätlingite.

Thermogravimetric analysis (TGA) of all samples after the second filtration, and selected samples after the first filtration, was carried out
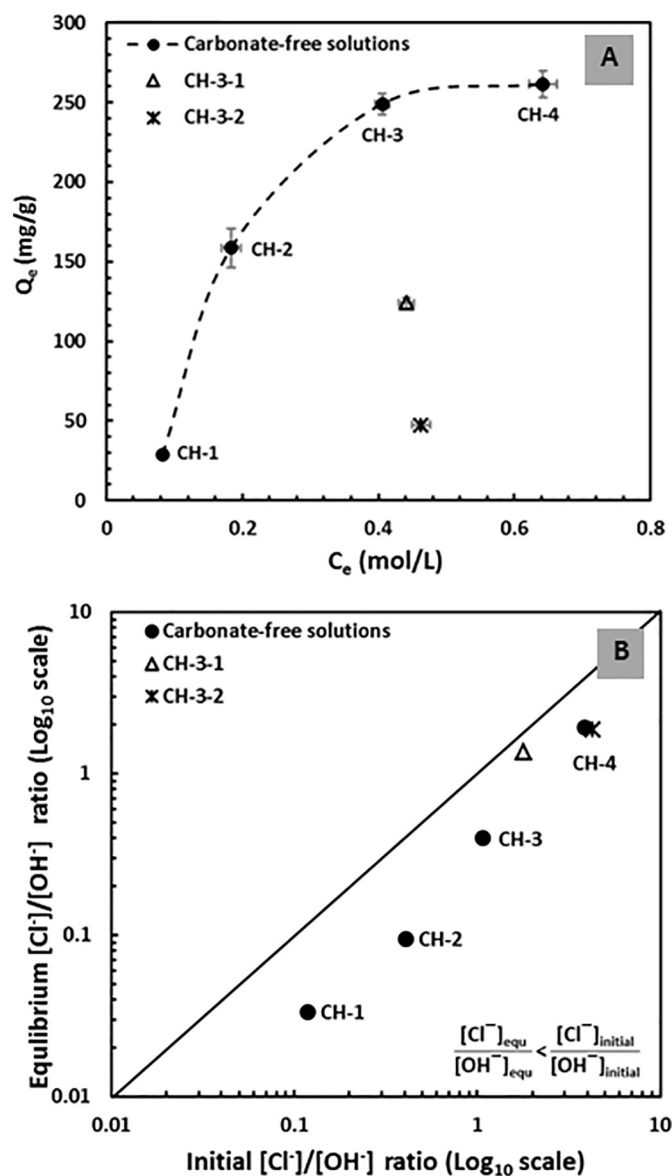

Fig. 1. (A) Chloride binding capacities of the Mg-Al LDH (calculated with respect to the mass of the CLDH used) in various chloride-rich simulated pore solutions, where the error bars correspond to one standard deviation among three replicates; (B) the $[Cl^-]/[OH^-]$ molar ratios at equilibrium vs. their initial values in each solution.

in a Perkin Elmer TGA 4000 instrument coupled with a Hiden mass spectrometer. In each case, 20 mg of sample was tested from 30 °C to 1000 °C at a heating rate of 3 °C/min, under nitrogen flowing at 20 mL/min.

3. Results and discussion

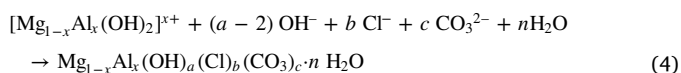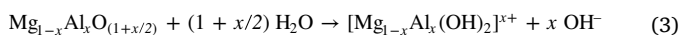### 3.1. Mg-Al hydrotalcite-like phase

3.1.1. Analysis of the supernatant before and after filtration

The initial and equilibrium chloride and hydroxide concentration values of two groups of the Cl-rich solution prior and after addition of CLDH solids were measured. The chloride binding capacity (Q_e) of the CLDH in each environment tested was calculated according to Eq. (2) (Fig. 1A). The $[Cl^-]/[OH^-]$ ratios at equilibrium in the measured solutions were plotted versus their initial $[Cl^-]/[OH^-]$ ratios (Fig. 1B). These values represent the total amount of free chlorides removed from the bulk solution per unit of CLDH solid, via both ion-exchange and surface adsorption in the solid CLDH, under various aqueous condi-

tions. The rehydration of the CLDH increased the alkalinity of the supernatant at equilibrium, even in these already highly alkaline solutions.

For the carbonate-free systems, where the equilibrium chloride concentrations ranged from 0 to 0.8 mol/L, the Q_e value increased significantly at increased $[Cl^-]/[OH^-]$ ratios, reaching a plateau above 0.5 mol/L initial chloride concentration (equivalent to $[Cl^-]/[OH^-]$ = 1) at around 250 mg Cl/g CLDH. Carbonated solutions CH-3-1 and CH-3-2 contained the same initial chloride concentration as solution CH-3; however, the equilibrium chloride concentrations in these two solutions are much higher than that of solution CH-3. This indicates a reduction in chloride binding capacities in the solid phase when carbonate is present. Between the two carbonated samples, the chloride binding capacity in solution CH-3-2 is lower than that in solution CH-3-1.

The reaction between CLDH and chloride rich solutions through exchange of interlayer species could be conceptualised as a two-step process: (i) hydrolysis of the dehydrated CLDH to form its layered double hydroxide structure with Mg and Al in the positively charged metal oxide sheet (Eq. (3)) [51], followed by (ii) intercalation of anions available in the liquid phase as interlayer species (Eq. (4)) [52]. Therefore, the availability of different types and concentrations of ions in the aqueous solution has a detrimental effect on the solid phase at equilibrium. In reality these processes will not necessarily be consecutive, as it is possible for some chloride to act directly in the re-formation of the LDH structure from the anhydrous material, but conceptualisation in this way does assist in assigning the contributions of different binding mechanisms. A higher initial $[Cl^-]/[OH^-]$ ratio, and the absence of carbonate, favour the uptake of chloride ions over hydroxide ions via the law of mass action, leading to determination of a higher Q_e value at higher chloride content. The plateau at high aqueous chloride concentration represents saturation of the available sites in the LDH material (interlayer and external surface) with chloride ions.

$$Mg_{1-x}Al_xO_{(1+x/2)} + (1 + x/2)\,H_2O \rightarrow [Mg_{1-x}Al_x(OH)_2]^{x+} + x\,OH^- \quad (3)$$

$$[Mg_{1-x}Al_x(OH)_2]^{x+} + (a - 2)\,OH^- + b\,Cl^- + c\,CO_3^{2-} + n\,H_2O$$
$$\rightarrow Mg_{1-x}Al_x(OH)_a(Cl)_b(CO_3)_c \cdot n\,H_2O \quad (4)$$

where $(a - 2) + b + 2c = x$.

In carbonated solutions, since the positively charged metal oxide sheets have stronger affinity for multivalent ions than monovalent ions [36,52], the carbonate ion is more competitive than both chloride and hydroxide ions as an interlayer species. The incorporation of carbonate in hydrotalcite-like phase would reduce the available chloride binding sites, thus resulting in lower Q_e values, even at the same initial chloride concentration and a higher initial $[Cl^-]/[OH^-]$ ratio. This suggests that the greatly reduced chloride binding capacity determined in solution CH-3-2 could be caused by the incorporation of carbonate ions into the interlayers due to a reduced hydroxide concentration.

The chloride uptake capacity of the Mg-Al LDH via surface adsorption is clearly important, as a mass balance calculation shows that the mass of chloride taken up by the LDH structure exceeds the quantity which could realistically be accommodated in interlayer sites. However, quantification of the partitioning of chlorides between the interlayer and the surface requires determination of the chemical composition of the solid phase after chloride binding; this will be discussed in detail in the following sections.

3.1.2. Chemical analysis of the solid Mg-Al LDH products

The elemental analysis of the solid material obtained after the first and second filtrations is reported in Table 2. In solid samples after the second filtration, the detected percentages of sodium and chloride were much lower than the values obtained after the first filtration, by as much as a factor of 10 for chloride in particular.

The Mg/Al ratios of the recrystallised LDH ranged from 2.0 to 2.3

(Table 2), similar to that of the original CLDH, except for the Mg/Al ratio detected from sample CH-4 after the first filtration, which is lower than the lowest acceptable Mg/Al ratio in hydrotalcite-like phase [53]. A very high percentage of intermixed NaCl crystals (as is evidently the case here from the Na and Cl contents) would make the calculation of Mg/Al ratio in hydrotalcite-like phase less reliable, indicated as "null" in Table 2.

In the diffuse layer, both Cl^- and OH^- can act as counter-ions. When the initial $[Cl^-]/[OH^-]$ is lower than 1, OH^- is the dominate anions in the solution, resulting in a significant amount of OH^- retention in diffuse layers as well. Since OH^- would not be detected by XRF, the amount of Na detected would be much higher than the amount of Cl. This explains why all samples, except CH-4, presented an Na content significantly higher than that of the stoichiometric composition of NaCl.

3.1.3. X-ray diffraction analysis of the recrystallised Mg-Al LDH

Fig. 2 shows the XRD patterns of recrystallised LDH after the first (Fig. 2A) and second (Fig. 2B) filtrations. A hydrotalcite-like phase, as well as crystallised NaCl (Powder diffraction file (PDF) # 01–078-0751), were identified after the first filtration. The intensities of NaCl reflections in Fig. 2A increased with increasing chloride concentration in the bulk solution. However, NaCl crystals are not identified in any of the samples after the second filtration, and only the hydrotalcite-like phase was observed in solids after the second filtration (Fig. 2B).

The basal peak position of the hydrotalcite-like phase after first filtration was centred at 11.6°, although the intensities and widths of this peak varies for the hydrotalcite-like phases which recrystallised in solutions with different chloride concentrations (Fig. 2A). This is most likely associated with changes in the amount of bound chlorides interrupting the regularity of the layered structure. In carbonate-free solutions, the basal peak of the hydrotalcite-like phase was broader and less intense after chloride exposure compared to the material obtained by recrystallising the same CLDH in water (marked CLDH-H2O in Fig. 2B). This was more notable in solutions with high chloride concentrations. Changes in the basal peak shape but not position indicate that the average interlayer spacing in chloride-exchanged hydrotalcite-like phases remain largely unchanged on average, but variation between different unit cells becomes more marked with a higher chloride loading. In the carbonate-containing samples CH-3-1, the basal reflection peak of the CLDH is even more diffuse than that of the samples with the highest chloride loadings in carbonate-free systems. This suggests that the incorporation of carbonate ions in the interlayer might induce a greater degree of local disorder in the hydrotalcite-like phase, compared with chloride ions.

After the second filtration (Fig. 2B) the basal peak reflections shifted slightly towards lower angle, while the peak shape stayed relatively unchanged. The shift in the basal peak reflection is attributed to either changes in the value of x ($x = Al / (Mg + Al)$) or different combinations of interlayer species [18,52]. Fig. 3 plots the basal peak positions (c' parameter, Å), as shown in Fig. 2B, of hydrotalcite-like phases prepared in this study against the x value calculated from Table 2. Regardless of the variation in the interlayer species and water content, it seems that the changes in basal peak positions of the hydrotalcite-like samples prepared in this study are mainly influenced by the x values, consistent with observations from the literature [52–57], and the lattice parameters deduced from the crystal geometries as proposed by Richardson [58,59].

Nevertheless, comparing data from this study with fully hydroxylated [52,54,55], fully carbonated [52,53,56,57], and chloride-exchanged hydrotalcite-like phases [18,52,60], different interlayer species do appear to influence the lattice parameters of the hydrotalcite-like phase differently. As shown in Fig. 3, fully hydroxylated hydrotalcite-like phases in general showed lower c' values; while chloride-exchanged hydrotalcite-like phases (with trace carbonate ions as interlayer species) were reported with higher c' values. The c' values for carbonated hydrotalcite-like phases were slightly higher than those

Table 2
XRF results for the solids obtained after the first and second filtration. Carbon is not detectable by the instrument used here. Data presented as elemental mass percentage.

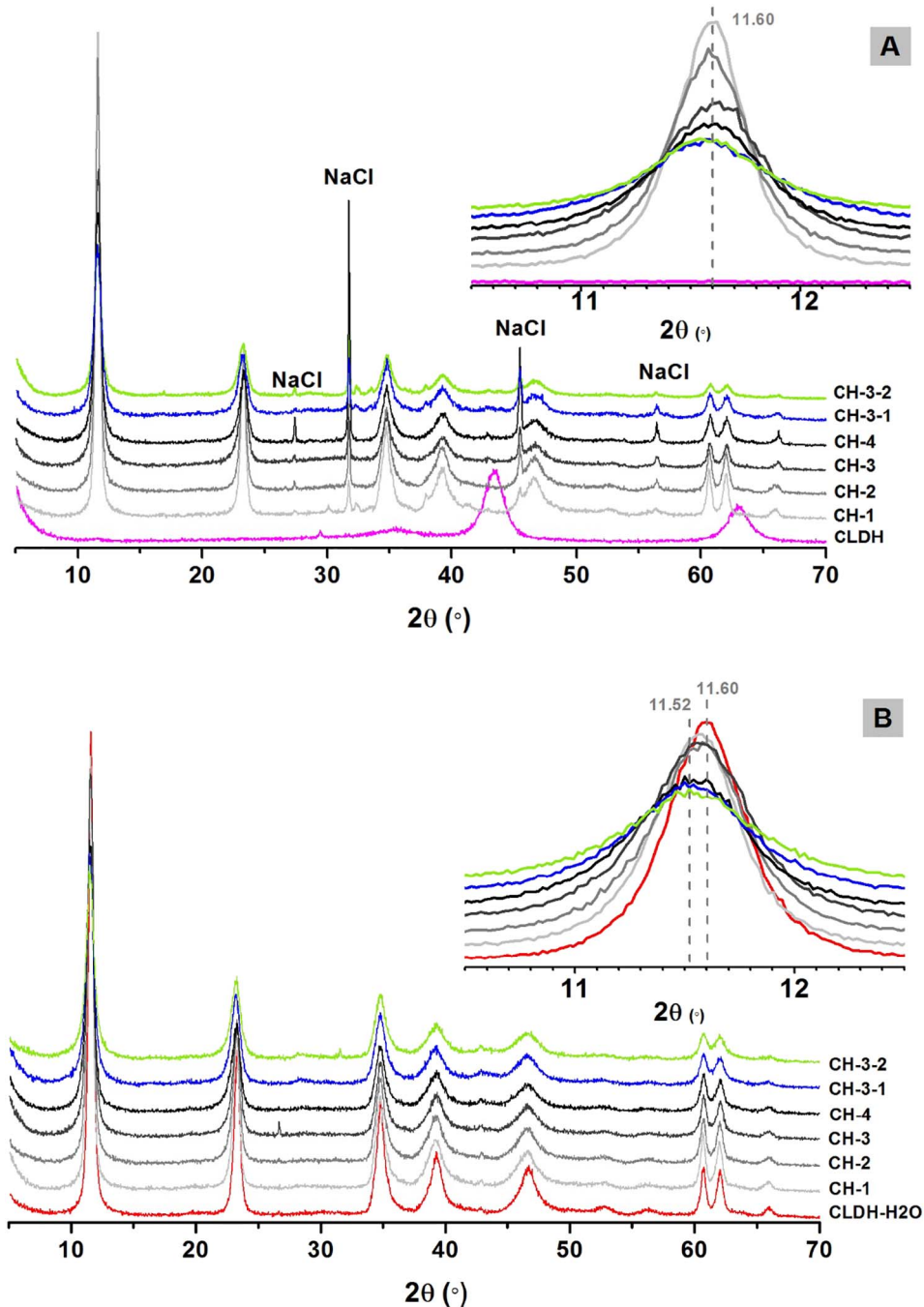| Elements	1st filtration				2nd filtration					
	CH-1	CH-2	CH-3	CH-4	CH-1	CH-2	CH-3	CH-4	CH-3-1	CH-3-2
Na	17.8	17.6	12.9	40.1	9.0	6.7	2.2	1.0	1.0	0.5
Cl	9.1	11.2	9.5	53.5	0.2	0.5	0.7	1.2	0.4	0.3
Mg	14.8	16.9	18.4	3.7	20.9	21.2	22.1	19.1	20.8	20.6
Al	8.2	8.8	9.1	2.6	11.5	10.9	11.8	9.5	11.0	10.5
O	50.1	45.4	50.1	n.d.[a]	58.4	60.7	63.2	69.1	66.8	68.2
Atomic ratio										
Mg/Al	2.0	2.1	2.3	Null	2.0	2.2	2.1	2.3	2.1	2.2

[a] n.d. represents "not detected".

Fig. 2. XRD patterns of recrystallised LDH in chloride-rich simulated pore solutions, (A) after the first filtration, with the pattern of the original CLDH; (B) after the second filtration, with the pattern of the CLDH recrystallised in distilled water (CLDH-H2O).
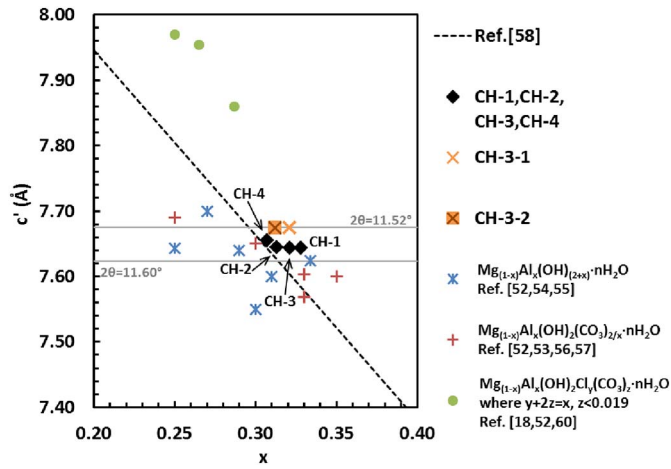
Fig. 3. The c' parameter plotted against x for Mg-Al hydrotalcite-like phases prepared in this study after 2nd filtration (Fig. 2B), together with fully hydroxylated, fully carbonated, and chloride-exchanged hydrotalcite-like phases reported in the literature. $Mg_{(1-x)}Al_x(OH)_{(2+x)} \cdot nH_2O$ data are from [52,54,55] and this study ($x = 0.33$); $Mg_{(1-x)}Al_x(OH)_2(CO_3)_{2/x} \cdot nH_2O$ data are from [52,53,56,57]; and $Mg_{(1-x)}Al_x(OH)_2Cl_y(CO_3)_z \cdot nH_2O$, where $y + 2z = x$, $z < 0.019$, data are from [18,52,60]. The dashed line was adopted from [58] as a guideline. The c' parameters presented here were obtained using the basal diffraction peak d_{003}, either directly from diffraction patterns (samples from this study) or the literature.

of the fully hydroxylated ones. The ionic radii of the interlayer species play influential roles here [52], as do the H-bonding networks which are formed with the ionic species. In aqueous solutions, one Cl^- can accept about 6 hydrogen bonds, 4 of which are from the surrounding water molecules [61]. This might explain the much larger interlayer spacing reported in the literature for chloride-exchanged hydrotalcite-like phases. The differences in the interlayer water content of the data discussed here should also be considered, and a $H_2O/(Mg + Al)$ ratio of 0.3–0.7 was reported in the literature as shown in Fig. 3; however no systematic deviations of water content between different samples were identified or specified in the plot.

The solid phase obtained after the first filtration contains chloride chemically or electrostatically bound in the interlayer, as well as chloride adsorbed to the diffuse electrical double layer (EDL) through surface adsorption. For ions retained in the diffuse layer, the total ion uptake is proportional to the capacity of the EDL (C_{EDL}, Eq. (5)), and closely related to the total ionic strength (I, Eq. (7)) in the solution (via Debye length λ_D, Eq. (6)) [62,63].

$$C_{EDL} = \frac{\varepsilon \varepsilon_0}{\lambda D} \tag{5}$$

$$\lambda_D = \sqrt{\frac{\varepsilon \varepsilon_0 kT}{2 N_A e^2 I}} \tag{6}$$

$$I = \frac{1}{2} \sum_i C_i Z_i^2 \tag{7}$$

ε - dielectric constant (relative permittivity), C/V·m.
ε_0 - permittivity of free space, C/V·m.
k - Boltzmann's constant, J/K.
T - temperature, K.
N_A - Avogadro's number, mol^{-1}.
e - elementary charge, C.
C_i - concentration of the ith ion, mol/L.
Z_i - valence of the ith ion.

It was previously identified [36,37] that chloride ions tend to become sorbed in the diffuse layer at the external surface of hydrotalcite-like phases, pairing with Na^+. A higher chloride concentration coupled with a lower hydroxide concentration will increase the thickness of the diffuse layer (i.e. the Debye length) on the outer surface of the hydrotalcite-like phase, increasing the capacity of the electrical double layer (Eq. (5)), and promoting the uptake of both sodium and chloride ions from the bulk solution [63]. For the samples obtained after the first filtration, the Na^+-Cl^- ion pairs in the diffuse layers crystallise to form NaCl upon drying (Fig. 2A). After the second filtration, the diffuse layer was diluted by the milli-Q water (ionic strength approaching 10^{-7} mol/L), so that the amount of chloride bound in the diffuse layer should become negligible. The remaining chloride identified in the solid phase by XRF (Table 3) should thus be considered to be interlayer species bound to the metal hydroxide layers.

In contrast to chloride ions, carbonate ions are linked to the metal hydroxyl layer of hydrotalcite-group minerals via H-bonding [64,65]. Binding of carbonate ions neutralises the interlayer acid hydroxyl groups, lowers the charge density of the surface (and so reduces the thickness of the diffuse layer), and thus limits the chloride uptake [36,63]. Hydroxide also bonds to the interlayer through H-bonding, and so there is direct competition between these ions; the relative bound concentrations will thus depend on the hydroxide concentration of the aqueous solution. A higher degree of carbonate ion-exchange in the interlayers leads to further reduction in surface charge density [36], and a reduced chloride uptake in the diffuse layer as a result. This is demonstrated by the low intensities of the reflections of NaCl crystals identified in Fig. 2A, for the carbonate-containing samples CH-3-1 and CH-3-2.

3.1.4. Thermogravimetric analysis of the solid CLDHs

Fig. 4 shows the TG-MS data for the solid phase after second filtration. The weight loss between room temperature and 228 °C is assigned to loss of chemically bound water (including surface water and interlayer water molecules) [66,67], and weight loss between 228 and 550 °C is due to both dehydroxylation of metal hydroxyl layers, and decarbonation of carbonate ions bonded to the metal hydroxyl layers present in a hydrotalcite-like structure [68,69].

The loss of chemically bound water from recrystallised Mg-Al LDH is a multi-step process. In carbonate-free systems, two water loss peaks appear: an intense and sharp peak at centred at 161 °C, the sharpness of
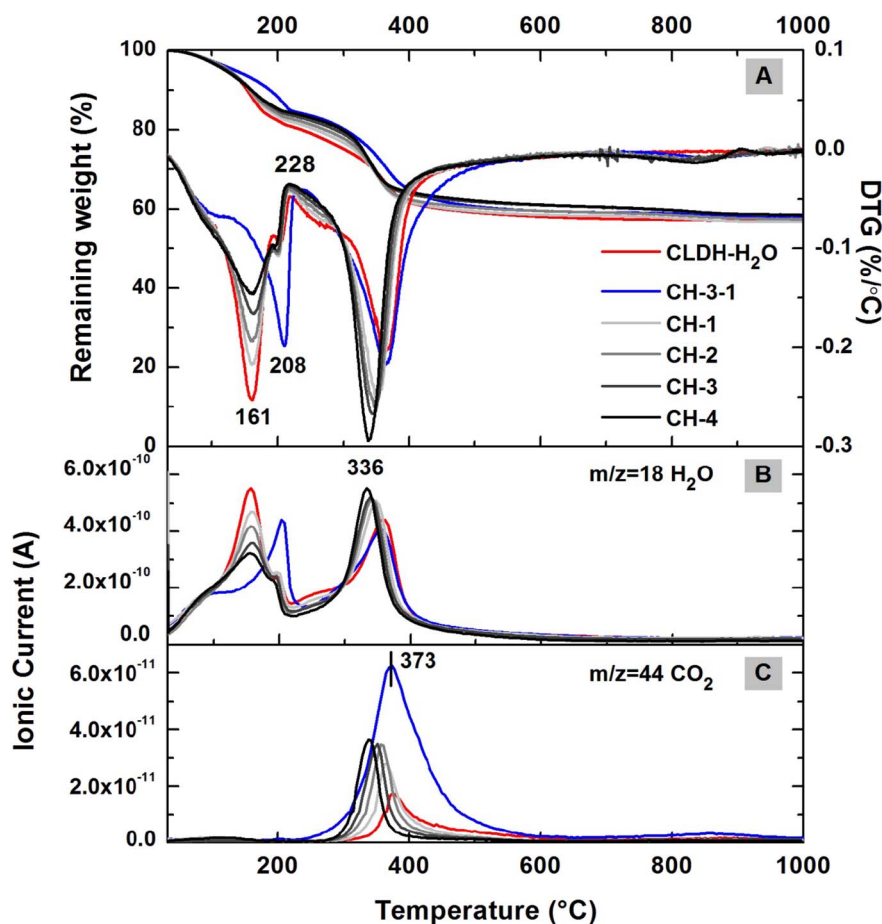
Table 3
Chemical compositions of recrystallised Mg-Al LDH after the second filtration, after equilibration under different conditions.

	General formulation: $Mg_{(1-x)}Al_x(OH)_a(Cl)_b(CO_3)_c \cdot nH_2O$	q_{e-Cl} (mg/g)[a]	Q^*_{e-Cl} (mg/g CLDH)[b]	$Q_e - Q^*_{e-Cl}$ (mg/g CLDH)
CH-1	$Mg_{0.672}Al_{0.328}(OH)_{2.272}(Cl)_{0.004}(CO_3)_{0.026} \cdot 0.985H_2O$	1.7	3.3	25.4
CH-2	$Mg_{0.687}Al_{0.313}(OH)_{2.262}(Cl)_{0.011}(CO_3)_{0.020} \cdot 0.929H_2O$	4.8	9.0	149.6
CH-3	$Mg_{0.679}Al_{0.321}(OH)_{2.265}(Cl)_{0.014}(CO_3)_{0.021} \cdot 0.888H_2O$	6.1	11.5	237.6
CH-4	$Mg_{0.693}Al_{0.307}(OH)_{2.233}(Cl)_{0.031}(CO_3)_{0.022} \cdot 0.855H_2O$	13.6	25.3	236.2
CH-3-1	$Mg_{0.679}Al_{0.321}(OH)_{2.100}(Cl)_{0.010}(CO_3)_{0.105} \cdot 0.819H_2O$	4.3	8.2	115.9
CH-3-2	$Mg_{0.688}Al_{0.312}(OH)_{2.071}(Cl)_{0.007}(CO_3)_{0.117} \cdot 0.826H_2O$	3.0	5.7	41.7

[a] q_{e-Cl} represents the mass fraction of interlayer Cl in recrystallised Mg-Al LDH, according to the chemical formula shown in the second column.
[b] Q^*_{e-Cl} represents the fraction of Cl, expressed relative to the mass of the CLDH ($Mg_{0.7}Al_{0.3}O_{1.15}$), assuming that one mole of input CLDH forms one mole of the recrystallised Mg-Al LDH shown in the second column. The changes in Mg and Al contents of the recrystallised hydrotalcite-like phase comparing with the input CLDH are < 3%, and therefore were not taken into account for calculation of Q^*_{e-Cl}.

Fig. 4. Thermogravimetry curves (A); and mass spectra of (B) H_2O ($m/z = 18$), and (C) CO_2 ($m/z = 44$), of recrystallised MgAl LDH immersed in various chloride rich simulated pore solutions, after the second filtration. Reference data for the thermally treated hydrotalcite (CLDH) immersed in milli-Q water (CLDH-H_2O) are also reported.
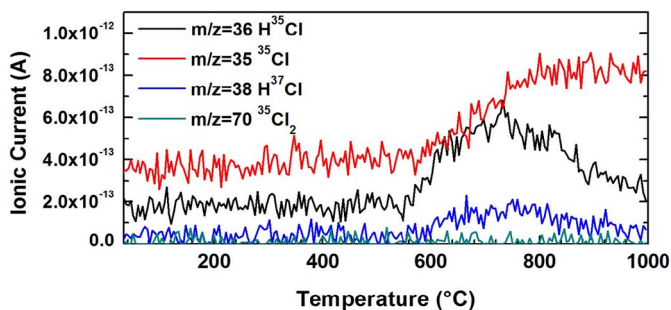

Fig. 5. Mass spectra of all Cl-containing gases released during thermogravimetric analysis of sample CH-3 after the second filtration.

which decreases with increased chloride concentrations in the solution, followed by a small peak centred at 208 °C, the intensity of which stays relatively unchanged across the samples immersed in solutions with different chloride concentrations. In samples immersed in the carbonate-containing solution CH-3-1, only a small shoulder at around 161 °C is observed, along with a high intensity peak at 208 °C.

The interlayer water molecules are also bound to the LDH structure through H-bonding, although with a binding energy lower than those of carbonate and hydroxide ions. In the carbonate- and chloride-free sample (Fig. 4; CLDH-H_2O), the only interlayer species are hydroxide and water, as well as trace carbonates. The H-bonding environment surrounding the interlayer water molecules in this sample (CLDH-H_2O) is more ordered [68]; therefore a sharp and strong water loss peak was identified at 161 °C. It is likely that an increased chloride concentration in the LDH interlayer induces an increase in the average H-bonding

energy for water molecules, as the chloride ions add attraction to water molecules through H-bonding [61]. With a higher content of interlayer carbonate, as in CH-3-1, the H-bonding network would be more complex, thus a higher temperature is required for the interlayer water to be removed (Fig. 3A) [68]. This is consistent with the XRD results (Fig. 2), where broader basal reflections were identified in samples with more complex interlayer species.

In Fig. 4C, a single CO_2 release peak was identified in all samples between 373 and 400 °C. In samples where carbonate ions were not added to the solution, the CO_2 release peak indicates some CO_2 contamination, probably caused during the sample separation or drying process. However, the amounts of carbonate which became incorporated in these samples without added carbonate samples were comparable across all samples.

Fig. 5 shows the mass spectra of all the chlorine-containing gases released during the thermal analysis process. The identification of loss of chlorine during thermogravimetric analysis is complicated by its low content in the solid phase, as well as the presence of different Cl isotopes [70]. However, Fig. 4 indicates that the weight loss contributed by release of chlorine from the solid phase takes place above 600 °C.

Table 3 summarises the chemical formulae of the hydrotalcite-group solids obtained after the second filtration from each solution studied, showing the compositions of interlayer species (OH^-, Cl^-, and CO_3^{2-}), calculated based on the XRF results and TG-MS data. The determination of chemical formulae was carried out assuming that the loss of chemical bounded water, including surface water and interlayer water molecules took place only between room temperature and 228 °C, the loss of hydroxyl groups and interlayer carbonates between 228 °C and 550 °C,

and the loss of chlorine-containing gases above 600 °C. It should be noted that the chemically bound water contents reported in Table 3 are calculated from analysis of each sample, and comprise both surface water and interlayer water molecules. The existence of some surface water was expected, as all solid samples were dried under controlled relative humidity (30 ± 3%) at room temperature.

The reduction in interlayer hydroxyl groups with increased interlayer chloride and carbonate ions is consistent with the discussion in Section 3.1.1 regarding the ion-exchange mechanism. In sample CH-4, where a maximum chloride uptake (from the bulk solution) of 262 mg/g was calculated, the interlayer chloride takes only 10% of the available anion sites. Reduced interlayer chloride contents were identified in samples that were immersed in carbonated solutions (CH-3-1 and CH-3-2). The carbonate contamination in all non-carbonate added samples is almost constant, about 12% of the maximum carbonate uptake by the LDH. In samples with 0.1 mol/L carbonate ions added to the bulk solution, the interlayer carbonate ions reached about 73% of the maximum carbonate capacities.

The Q^*_{e-Cl} values shown in Table 3 correspond to the weight percentage of interlayer chloride in the hydrotalcite-like phase (expressed on the basis of the initial mass of CLDH), which are 5–10% of the Q_e values reported in Fig. 1A. The amount of chloride taken up by the rehydrated CLDH via surface adsorption, the final column in Table 3, is calculated by subtracting Q^*_{e-Cl} calculated from the solid phase from Q_e calculated from the aqueous solutions. Chloride uptake by Mg-Al LDH phases via surface adsorption is influenced by the chemical binding capacity of the diffuse electrical double layer in each sample.

3.2. AFm phase - strätlingite

Fig. 6 shows the chloride uptake of strätlingite immersed in solutions with different chloride concentrations, and the $[Cl^-]/[OH^-]$ ratio in equilibrium solution in comparison with initial $[Cl^-]/[OH^-]$ ratios. The chloride uptake capacities of strätlingite under different aqueous conditions were also calculated using Eq. (2).

Similar to the trends identified for the Mg-Al LDH (Fig. 1A), for carbonate-free solutions the total chloride uptake capacity of the AFm phase rises as the $[Cl^-]/[OH^-]$ ratio increases. The chloride binding capacity of strätlingite is higher than that of Mg-Al LDH at lower initial $[Cl^-]/[OH^-]$ ratio (< 0.3), but lower at higher initial $[Cl^-]/[OH^-]$ ratios (> 0.3). The maximum chloride binding capacity achieved was about 204 mg/g, at an initial $[Cl^-]/[OH^-]$ ratio of 3. The differences in the chloride binding isotherm of strätlingite, compared with that of Mg-Al LDH (Fig. 1A), suggest that the interaction between chloride ions and strätlingite might involve different binding mechanisms, most likely a lattice substitution [30,71]. The decrease in chloride uptake by strätlingite induced by an increased $[CO_3^{2-}]/[OH^-]$ ratio is similar to that identified for the hydrotalcite-like phase, although less significant changes were observed in the chloride uptake from solutions CH-3-1* and CH-3-2* compared with the sample CH-3* in strätlingite, compared to the identified for Mg-Al LDH. It is possible that the decreased chloride binding capacity of strätlingite in carbonated solutions is due to the formation of carbonated AFm phases, such as hemicarbonate or monocarbonate [30]. This will be examined in detail in the following sections.

Fig. 7 shows the XRD patterns of strätlingite after being immersed in chloride-rich solutions. Distinctive peaks assigned to crystallised NaCl were identified in the solid phase after the first filtration, where the Na$^+$ and Cl$^-$ ions are still retained in the diffuse layer. Similar to the case identified for the hydrotalcite-like phase (Fig. 2), the intensities of the NaCl reflections in Fig. 6 decrease with a reduced initial $[Cl^-]/[OH^-]$ ratio. Minor traces of NaCl are identified in sample CH-1* (Fig. 7A). As discussed above, the reduced $[Cl^-]/[OH^-]$ ratio (lower chloride concentration but higher NaOH content) results in a lower surface charge density and probably a thinner diffuse layer [63],
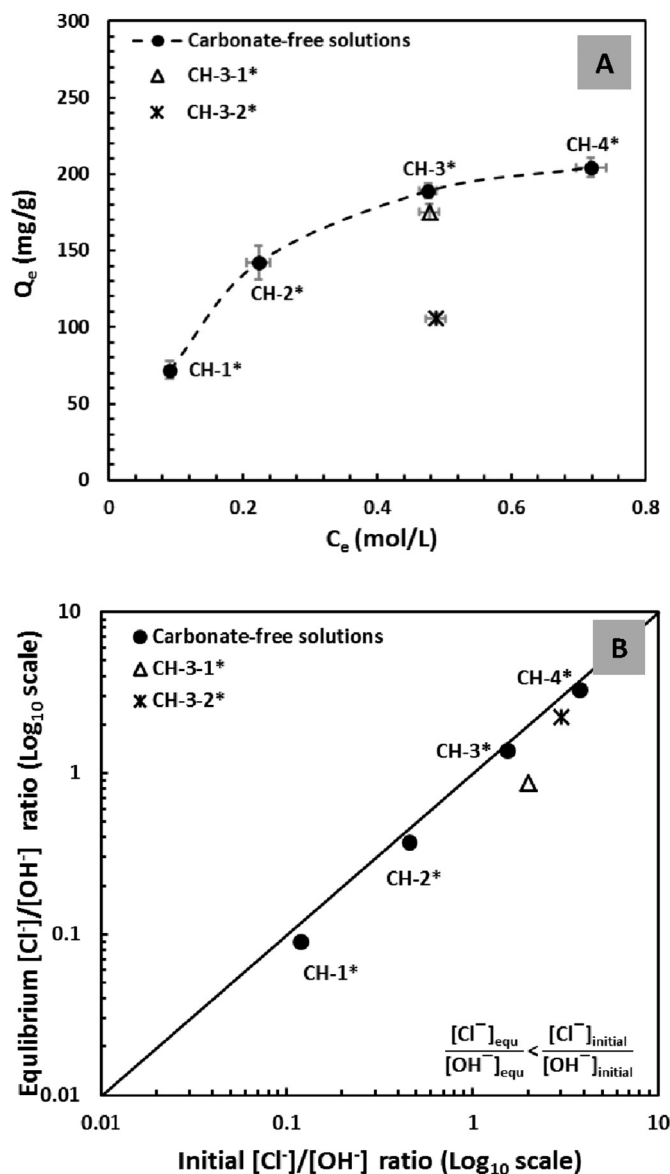

Fig. 6. (A) Chloride binding capacity of strätlingite in various chloride rich simulated pore solutions. Q_e calculated using Eq. (2), where the error bars indicate one standard deviation among three replicates; (B) the $[Cl^-]/[OH^-]$ molar ratios measured at equilibrium versus their initial values.

reducing the amount of chloride retained in the diffuse layer upon filtration.

A chloride-bearing AFm phase (AFm-Cl), with a crystal structure resembling the Cl-substituted hydrocalumite-type phase Friedel's salt ($Ca_2Al(OH)_6Cl·2H_2O$, PDF# 01–078-1219), was identified in samples immersed in the non-carbonated chloride rich solutions. Only part of the strätlingite converted to Friedel's salt though ion-exchange, as residual strätlingite reflections were identified along with the chloride bearing AFm phase, and the correspondence between the XRD data here and the reference PDF pattern for pure Friedel's salt is not exact. In the presence of even a trace of carbonate ions in the system (Fig. 8C), the rhombohedral type polymorph of the Friedel's salt-like phase is formed rather than monoclinic Friedel's salt [72]. This indicates some degree of ionic substitution or disorder in the interlayers of this phase [30,72]. Although the positively charged layers in strätlingite, $CaAl_2(OH)_6{}^+$, are the same as in all the other AFm phases [48,73], the amount of ion-exchangeable hydroxyl sites bounded to the mixed metal sheets in strätlingite is much more limited [48]. Also, for full replacement of the complex interlayer aluminosilicate ion species, [AlSi
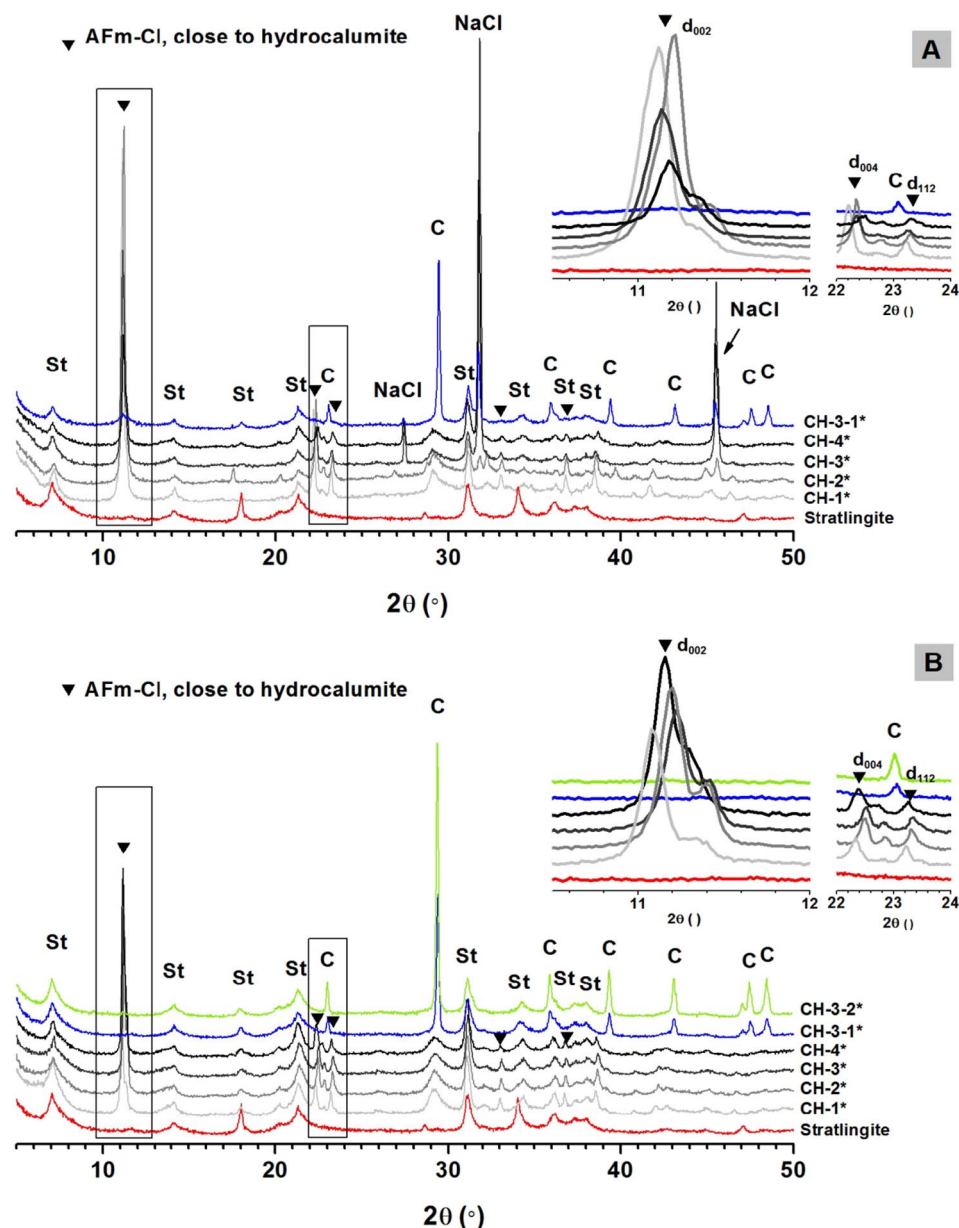
Fig. 7. XRD pattern of strätlingite after interaction with chloride rich simulated pore solutions, (A) after first filtration; (B) after second filtration. Insets in each case show expansions of the regions highlighted with rectangles, where C refers to calcite, St refers to strätlingite.

$(O_8H_8) \cdot 0.25H_2O]^-$, a higher chloride concentration or ionic strength might be required.

In the strätlingite immersed in the carbonate-free solutions, the chloride bearing AFm-phase formed has a $d_{(002)}$ spacing ranging from 7.88 Å to 7.98 Å (inset in Fig. 7). The shift of the basal peak position in hydrocalumite-like AFm phases is correlated to the composition of the interlayer anions, as well as interlayer water [71]. However, the intensities of hydrocalumite basal peaks are not linearly related to the Cl content in the interlayers.

In samples immersed in carbonated solutions, calcite ($CaCO_3$, PDF# 00-005-0586) was identified as a reaction product. Chloride bearing AFm-phases were not observed in these specimens. This is probably associated with the decomposition of the hydrocalumite-like phase upon carbonation, as proposed by Anstice et al. [74]. However, the existence of a disordered ('X-ray amorphous') AFm(CO_3, Cl) solid solution is also plausible. When keeping the chloride concentration and carbonate concentrations constant, but decreasing the OH⁻ concentration from 0.3 mol/L to 0.1 mol/L (i.e. moving from system CH3–1* to CH3–2*), the amount of calcite increased significantly, most

likely suggesting the extraction of calcium from strätlingite to form calcite in the presence of dissolved carbonate were favoured at slightly lower OH⁻ concentrations. However, it should be noted that, even though sample CH3–2* has the lowest alkalinity after equilibrium, the measured pH values was 13.4. Strätlingite is normally considered as stable at pH higher than 13 in the absence of carbonate ions in the aqueous phase [75]. There is not sufficient evidence from this study to explain the decalcification of strätlingite at this high pH, however the role of carbonate in the aqueous phase should be emphasised.

Fig. 8 shows the TG-MS data obtained for solid AFm samples after the second filtration, in comparison with the synthetic strätlingite. For the synthetic strätlingite, the chemically bound interlayer water was lost at around 145 °C, and the structural hydroxyl groups were decomposed before 250 °C [75,76]. There are two small CO_2 release peaks observed in the CO_2 mass spectra (Fig. 8C), centred at 400 °C and 800 °C, respectively. This is consistent with the decarbonation of minor interlayer carbonate ions in strätlingite, and/or decomposition of sodium carbonate [77]. The formation of these carbonate-containing
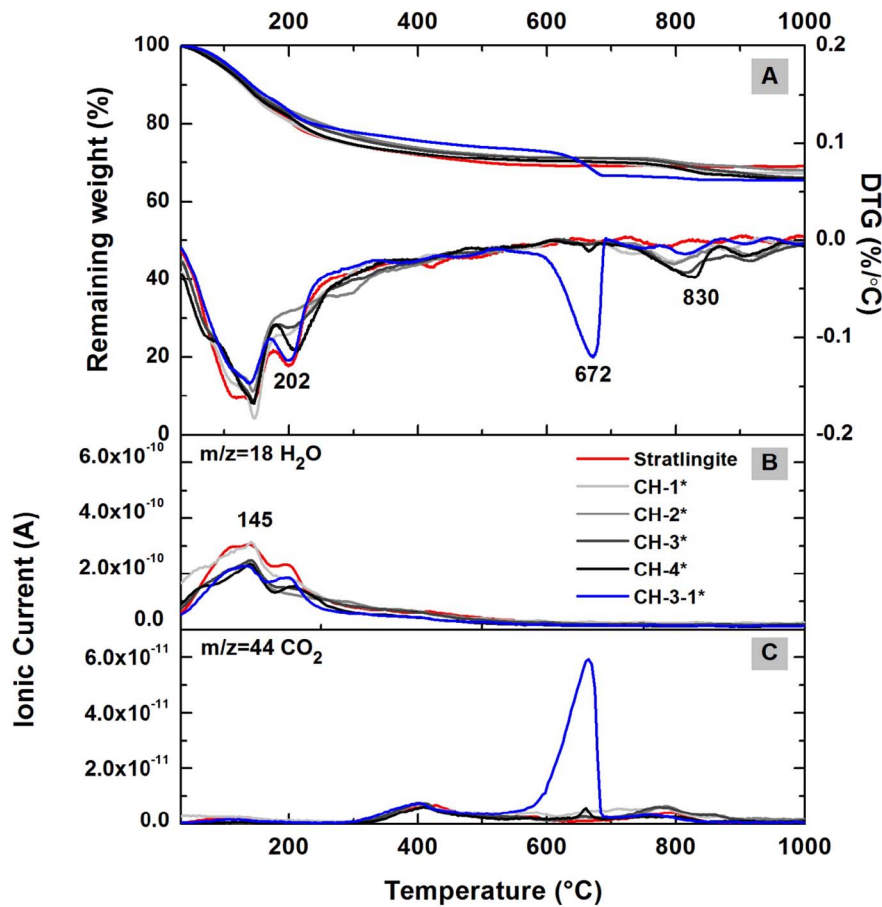
Fig. 8. Thermogravimetry curves (A); and mass spectra of (B) H$_2$O ($m/z = 18$), and (C) CO$_2$ ($m/z = 44$), for strätlingite immersed in various chloride rich simulated pore solution, after the second filtration. Reference results for the synthesised strätlingite are also reported.
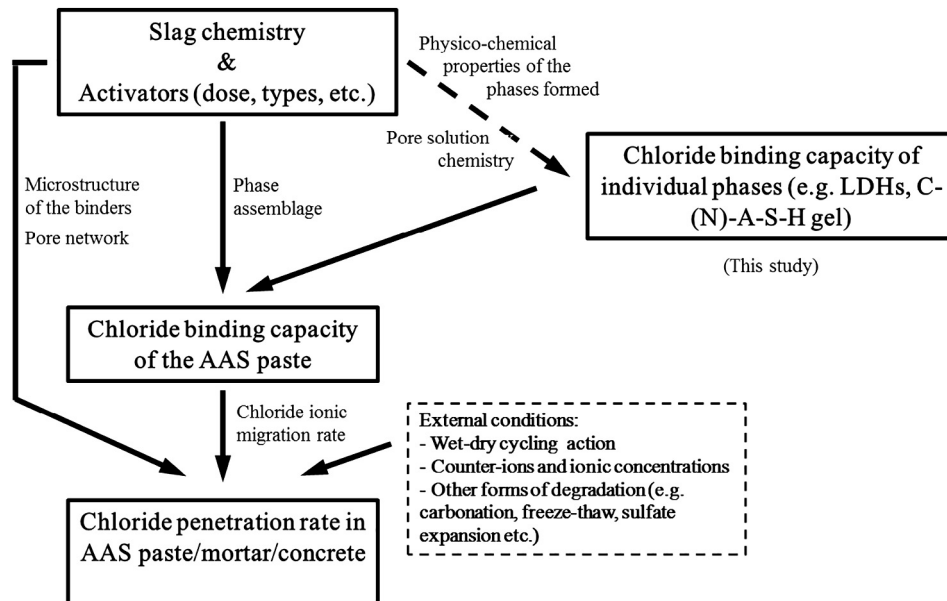

Fig. 9. Illustration of some of the factors which control chloride transport in AAS.

phases is attributed to CO$_2$ contamination during the sample preparation process. It has been reported that strätlingite accommodates a small amount of carbonate ions as interlayer species without significant changes in its crystal structure [48]. Combining the MS data for CO$_2$ (Fig. 8C) with the TG data (Fig. 8A), a total CO$_2$ contamination in the input strätlingite of < 1.0 wt% was calculated.

The mixture of strätlingite and hydrocalumite-like phases in the solid samples after the second filtration makes the interpretation of the thermogravimetry results challenging. No significant changes in samples immersed in chloride-rich solution are observable from the TG-MS results, apart from minor shifts in the dehydroxylation peaks at around 202 °C and weight loss peaks at around 830 °C. For samples prepared in

carbonate-free solution, less intense dehydroxylation peaks were observed for samples with lower chloride content. In contrast to the trends identified for Mg-Al LDH (Fig. 4), there is not a clear trend of changes in the dehydration/dehydroxylation peak intensity and/or width in chloride-bearing strätlingite. This is possibly due to its more complex interlayer structure. The weight loss at around 830 °C seems to relate to the releasing of chlorine-containing gases, as the intensity of the weight loss peak rises with increased chloride content in the solids.

Quantification of the amount of chloride bounded to the strätlingite via lattice substitution is complicated, considering the intimate intermixture of strätlingite with the newly-formed Friedel's salt-like phase after immersion in chloride-rich simulated pore solutions. However, in aiming to enable estimation of chloride binding capacity for known phase assemblages in alkali-activated binders, this study has provided very valuable information regarding estimation of chloride uptake by strätlingite, as shown in Fig. 6. The amount of chloride taken up through surface adsorption would be more sensitive to changes in the aqueous environment, while the formation of the chloride-AFm solid solution is relatively more stable as the chloride bearing phase.

4. Implication for the chloride binding capacity of alkali-activated slag materials

Fig. 9 illustrates the different factors which contribute to controlling the rate of transport of chloride in alkali-activated slag materials. In the first instance, the phase assemblage of these materials and the chloride binding capacity of each of the individual phases forming will play a key role in the mitigation of chloride penetration.

The pH value of the pore solution in alkali-activated slag cement is expected to change during exposure to a near-neutral external chloride source, like sea water or de-icing salt solution, due to alkali leaching from the pore network. The $[Cl^-]/[OH^-]$ ratios will also be influenced by this characteristic, and this may in fact give both buffering and additional binding capacity for chloride, as the hydroxide bound in the LDH phases formed during the hydration of the binder can be released and replaced by incoming chloride.

The results presented in this study show that the binding capacity of LDHs changes as a function of the $[Cl^-]/[OH^-]$ ratios, implying that the chloride binding capacity of these phases will differ at different depth of chloride penetration into a hardened monolithic specimen. The $[Cl^-]/[OH^-]$ ratios in the pore solution is likely to increase over time, resulting in high chloride uptake, until the LDHs reach their maximum chloride uptake capacity. This process is expected to significantly retard the ingress of chloride, and is a key factor underlying the observed slow movement of chloride through alkali-activated concretes compared to Portland cement concretes, of comparable total pore volume [5–7]. From Figs. 1A and 6A, it can be estimated that the maximum chloride uptake capacities of the hydrotalcite-like phase and strätlingite are about 250 mg/g and 200 mg/g, respectively, even at $[Cl^-]/[OH^-]$ ratios higher than 3.

Hydrotalcite-group minerals are well known as effective chloride binding phases, contributing to the low chloride penetration rate of cementitious materials containing slag as a main binder material [32,78]. This study has illustrated that, in chloride-rich simulated alkali-activated slag pore solutions, most of the chlorides are taken up by hydrotalcite-like phases through surface adsorption in the diffuse layer rather than through direct ion-exchange. However, since the mobility of chlorides in the diffuse layer is much slower than that in the bulk solution, a high contribution from surface adsorption may effectively slow down the ingress of free chlorides in the cement matrix [79,80]. Similarly, the binding of chlorides in the AFm phases which can form within alkali-activated slag binders also offers significant scope for restriction of chloride movement.

5. Conclusions

This study reports for the first time the chloride binding capacities, under high alkalinity conditions, of the hydrotalcite-like (Mg-Al) and strätlingite (AFm) layered double hydroxides which are identified as reaction products in many Portland blended cements and alkali-activated slag cements. It has been demonstrated that this hydrotalcite-like phase and strätlingite can effectively take up chloride from highly alkaline solutions with different initial $[Cl^-]/[OH^-]$ ratios. For a hydrotalcite-like phase, surface adsorption is the main binding mechanism, responsible for around 90% of the total chloride uptake, with around 10% contribution from ion exchange. For strätlingite, surface adsorption of chlorides is less dominant, and lattice substitution of chloride also takes place. Chloride uptake by hydrotalcite-like phases is sensitive to changes in the pH, chloride concentration and total ionic strength of the solution, more so than is the case for AFm phases.

The presence of carbonates in the pore solution, along with a decrease in the alkalinity of the system, significantly decreases the chloride uptake by both LDH mineral families. Carbonate in hydrotalcite-like phases will occupy the chloride-exchangeable interlayer hydroxyl sites and reduce surface adsorption, while in strätlingite it can participate in ion exchange, but also (when the aqueous environment is poor in aluminium) leads to partial decomposition of the AFm phase, inducing the precipitation of calcite instead.

The modification in the chloride binding capacities of hydrotalcite-like phase and strätlingite as a function of $[Cl^-]/[OH^-]$ ratio should be taken into consideration when building up a detailed model for prediction of chloride penetration profiles, as different chloride binding capacities will need to be applied when considering the changes in the pore fluid composition depending on depth from the surface of the sample.

Acknowledgements

References

[1] S. Goñi, C. Andrade, Synthetic concrete pore solution chemistry and rebar corrosion rate in the presence of chlorides, Cem. Concr. Res. 20 (1990) 525–539.

[2] F.P. Glasser, J. Marchand, E. Samson, Durability of concrete - degradation phenomena involving detrimental chemical reactions, Cem. Concr. Res. 38 (2008) 226–246.

[3] U. Angst, B. Elsener, C.K. Larsen, Ø. Vennesland, Critical chloride content in reinforced concrete — a review, Cem. Concr. Res. 39 (2009) 1122–1138.

[4] J.L. Provis, S.A. Bernal, Geopolymers and related alkali-activated materials, Annu. Rev. Mater. Res. 44 (2014) 299–327.

[5] I. Ismail, S.A. Bernal, J.L. Provis, R. San Nicolas, D.G. Brice, A.R. Kilcullen, S. Hamdan, J.S.J. van Deventer, Influence of fly ash on the water and chloride permeability of alkali-activated slag mortars and concretes, Constr. Build. Mater. 48 (2013) 1187–1201.

[6] Q. Ma, S.V. Nanukuttan, P.A.M. Basheer, Y. Bai, C. Yang, Chloride transport and the resulting corrosion of steel bars in alkali activated slag concretes, Mater. Struct. 49 (2015) 3663–3667.

[7] C. Shi, Strength, pore structure and permeability of alkali-activated slag mortars, Cem. Concr. Res. 26 (1996) 1789–1799.

[8] S.A. Bernal, R. Mejía de Gutiérrez, A.L. Pedraza, J.L. Provis, E.D. Rodríguez, S. Delvasto, Effect of binder content on the performance of alkali-activated slag concretes, Cem. Concr. Res. 41 (2011) 1–8.

[9] C.J. Shi, Effect of mixing proportions of concrete on its electrical conductivity and the rapid chloride permeability test (ASTM C1202 or ASSHTO T277) results, Cem. Concr. Res. 34 (2004) 537–545.

[10] Q. Yuan, C. Shi, G. De Schutter, K. Audenaert, D. Deng, Chloride binding of cement-

based materials subjected to external chloride environment – a review, Constr. Build. Mater. 23 (2009) 1–13.

[11] S.A. Bernal, R. San Nicolas, R.J. Myers, R. Mejía de Gutiérrez, F. Puertas, J.S.J. van Deventer, J.L. Provis, MgO content of slag controls phase evolution and structural changes induced by accelerated carbonation in alkali-activated binders, Cem. Concr. Res. 57 (2014) 33–43.

[12] M. Ben Haha, B. Lothenbach, G. Le Saout, F. Winnefeld, Influence of slag chemistry on the hydration of alkali-activated blast-furnace slag — part I: effect of MgO, Cem. Concr. Res. 41 (2011) 955–963.

[13] X. Ke, S.A. Bernal, J.L. Provis, Controlling the reaction kinetics of sodium carbonate-activated slag cements using calcined layered double hydroxides, Cem. Concr. Res. 81 (2016) 24–37.

[14] S.A. Bernal, J.L. Provis, A. Fernández-Jiménez, P.V. Krivenko, E. Kavalerova, M. Palacios, C. Shi, Binder chemistry–high-calcium alkali-activated materials, in: J.L. Provis, J.S.J. van Deventer (Eds.), Alkali-Activated Materials, State of the Art Report of RILEM TC 224-AAM, Springer/RILEM, Dordrecht, 2014, pp. 59–91.

[15] C. Andrade, M. Prieto, P. Tanner, F. Tavares, R. d'Andrea, Testing and modelling chloride penetration into concrete, Constr. Build. Mater. 39 (2013) 9–18.

[16] C. Arya, N.R. Buenfeld, J.B. Newman, Factors influencing chloride-binding in concrete, Cem. Concr. Res. 20 (1990) 291–300.

[17] X. Duan, D.G. Evans, Layered Double Hydroxides, Springer, Berlin Heidelberg, 2006.

[18] S. Miyata, The syntheses of hydrotalcite-like compounds and their structures and physico-chemical properties I: the systems Mg^{2+}-Al^{3+}-NO_3^-, Mg^{2+}-Al^{3+}-Cl^-, Mg^{2+}-Al^{3+}-ClO_4^-, Ni^{2+}-Al^{3+}-Cl^- and Zn^{2+}-Al^{3+}-Cl^-, Clays Clay Miner. 23 (1975) 369–375.

[19] T. Sato, H. Fujita, T. Endo, M. Shimada, A. Tsunashima, Synthesis of hydrotalcite-like compounds and their physico-chemical properties, React Solids 5 (1988) 219–228.

[20] M. Ben Haha, B. Lothenbach, G. Le Saout, F. Winnefeld, Influence of slag chemistry on the hydration of alkali-activated blast-furnace slag — part II: effect of Al_2O_3, Cem. Concr. Res. 42 (2012) 74–83.

[21] S.J. Mills, A.G. Christy, J.-M.R. Génin, T. Kameda, F. Colombo, Nomenclature of the hydrotalcite supergroup: natural layered double hydroxides, Mineral. Mag. 76 (2012) 1289–1336.

[22] R.J. Myers, B. Lothenbach, S.A. Bernal, J.L. Provis, Thermodynamic modelling of alkali-activated slag cements, Appl. Geochem. 61 (2015) 233–247.

[23] A.R. Brough, A. Atkinson, Sodium silicate-based, alkali-activated slag mortars: part I. Strength, hydration and microstructure, Cem. Concr. Res. 32 (2002) 865–879.

[24] J.I. Escalante-García, A.F. Fuentes, A. Gorokhovsky, P.E. Fraire-Luna, G. Mendoza-Suarez, Hydration products and reactivity of blast-furnace slag activated by various alkalis, J. Am. Ceram. Soc. 86 (2003) 2148–2153.

[25] I.G. Richardson, A.R. Brough, G.W. Groves, C.M. Dobson, The characterization of hardened alkali-activated blast-furnace slag pastes and the nature of the calcium silicate hydrate (C-S-H) phase, Cem. Concr. Res. 24 (1994) 813–829.

[26] F. Puertas, A. Fernández-Jiménez, M.T. Blanco-Varela, Pore solution in alkali-activated slag cement pastes. Relation to the composition and structure of calcium silicate hydrate, Cem. Concr. Res. 34 (2004) 139–148.

[27] J. Schneider, M.A. Cincotto, H. Panepucci, ^{29}Si and ^{27}Al high-resolution NMR characterization of calcium silicate hydrate phases in activated blast-furnace slag pastes, Cem. Concr. Res. 31 (2001) 993–1001.

[28] S.-D. Wang, K.L. Scrivener, ^{29}Si and ^{27}Al NMR study of alkali-activated slag, Cem. Concr. Res. 33 (2003) 769–774.

[29] S.A. Bernal, J.L. Provis, R.J. Myers, R. San Nicolas, J.S.J. van Deventer, Role of carbonates in the chemical evolution of sodium carbonate-activated slag binders, Mater. Struct. 48 (2014) 517–529.

[30] A. Mesbah, C. Cau-dit-Coumes, F. Frizon, F. Leroux, J. Ravaux, G. Renaudin, A new investigation of the Cl^--CO_3^{2-} substitution in AFm phases, J. Am. Ceram. Soc. 94 (2011) 1901–1910.

[31] A. Mesbah, C. Cau-dit-Coumes, G. Renaudin, F. Frizon, F. Leroux, Uptake of chloride and carbonate ions by calcium monosulfoaluminate hydrate, Cem. Concr. Res. 42 (2012) 1157–1165.

[32] O. Kayali, M.S.H. Khan, M.S. Ahmed, The role of hydrotalcite in chloride binding and corrosion protection in concretes with ground granulated blast furnace slag, Cem. Concr. Compos. 34 (2012) 936–945.

[33] O. Kayali, M.S. Ahmed, M.S.H. Khan, Friedel's salt and hydrotalcite – layered double hydroxides and the protection against chloride induced corrosion, Civil Environ. Res. 5 (2013) 111–117.

[34] Z. Yang, H. Fischer, R. Polder, Possibilities for improving corrosion protection of reinforced concrete by modified hydrotalcites – a literature review, in: C. Andrade, J. Gulikers (Eds.), Advances in Modeling Concrete Service Life, Springer, Netherlands, 2012, pp. 95–105.

[35] U.A. Birnin-Yauri, F.P. Glasser, Friedel's salt, $Ca_2Al(OH)_6(Cl,OH) \cdot 2H_2O$: its solid solutions and their role in chloride binding, Cem. Concr. Res. 28 (1998) 1713–1723.

[36] K. Morimoto, S. Anraku, J. Hoshino, T. Yoneda, T. Sato, Surface complexation reactions of inorganic anions on hydrotalcite-like compounds, J. Colloid Interface Sci. 384 (2012) 99–104.

[37] L. Châtelet, J.Y. Bottero, J. Yvon, A. Bouchelaghem, Competition between mono-valent and divalent anions for calcined and uncalcined hydrotalcite: anion exchange and adsorption sites, Colloids Surf. A Physicochem. Eng. Asp. 111 (1996) 167–175.

[38] M.S.H. Khan, O. Kayali, U. Troitzsch, Chloride binding capacity of hydrotalcite and the competition with carbonates in ground granulated blast furnace slag concrete, Mater. Struct. 49 (2016) 4609–4619.

[39] S. Yoon, J. Moon, S. Bae, X. Duan, E.P. Giannelis, P.J.M. Monteiro, Chloride adsorption by calcined layered double hydroxides in hardened Portland cement paste, Mater. Chem. Phys. 145 (2014) 376–386.

[40] S.V. Prasanna, P.V. Kamath, Anion-exchange reactions of layered double hydroxides: interplay between coulombic and H-bonding interactions, Ind. Eng. Chem. Res. 48 (2009) 6315–6320.

[41] D.J. Shaw, Introduction to Colloid and Surface Chemistry, Butterworth-Heinemann, London, 1992.

[42] M.V.A. Florea, H.J.H. Brouwers, Chloride binding related to hydration products: part I: ordinary Portland cement, Cem. Concr. Res. 42 (2012) 282–290.

[43] S. Song, H.M. Jennings, Pore solution chemistry of alkali-activated ground granulated blast-furnace slag, Cem. Concr. Res. 29 (1999) 159–170.

[44] M. Fernández Bertos, S.J.R. Simons, C.D. Hills, P.J. Carey, A review of accelerated carbonation technology in the treatment of cement-based materials and seques-tration of CO_2, J. Hazard. Mater. 112 (2004) 193–205.

[45] S.A. Bernal, J.L. Provis, D.G. Brice, A. Kilcullen, P. Duxson, J.S.J. van Deventer, Accelerated carbonation testing of alkali-activated binders significantly under-estimates service life: the role of pore solution chemistry, Cem. Concr. Res. 42 (2012) 1317–1326.

[46] T. Matschei, B. Lothenbach, F.P. Glasser, Thermodynamic properties of Portland cement hydrates in the system CaO–Al_2O_3–SiO_2–$CaSO_4$–$CaCO_3$–H_2O, Cem. Concr. Res. 37 (2007) 1379–1410.

[47] X. Ke, S.A. Bernal, J.L. Provis, S.A. Bernal, J.L. Provis (Eds.), Chloride binding behaviour of hydrotalcite in simulated chloride-rich pore solution, Proceedings of the 34th Cement and Concrete Science Conference, IoM^3, Sheffield, 2014.

[48] M.U. Okoronkwo, F.P. Glasser, Strätlingite: compatibility with sulfate and carbo-nate cement phases, Mater. Struct. 49 (2016) 3569–3577.

[49] ASTM International, ASTM D512-12, Standard Test Methods for Chloride Ion in Water, ASTM International, West Conshohocken, PA, 2012.

[50] RILEM TC 178-TMC, Recommendations of RILEM TC 178-TMC: testing and modelling chloride penetration in concrete analysis of water soluble chloride content in concrete, Mater. Struct. 35 (2002) 586–588.

[51] H. Tamura, A. Tanaka, K.-y. Mita, R. Furuichi, Surface hydroxyl site densities on metal oxides as a measure for the ion-exchange capacity, J. Colloid Interface Sci. 209 (1999) 225–231.

[52] S. Miyata, Anion-exchange properties of hydrotalcite-like compounds, Clays Clay Miner. 31 (1983) 305–311.

[53] M.C. Gastuche, G. Brown, M.M. Mortland, Mixed magnesium-aluminium hydro-xides I. Preparation and characterization of compounds formed in dialysed systems, Clay Miner. 7 (1967) 177–192.

[54] G. Mascolo, O. Marino, A new synthesis and characterization of magnesium-aluminium hydroxides, Mineral. Mag. 43 (1980) 619–621.

[55] S. Koritnig, P. Süsse, Meixnerit, $Mg_6Al_2(OH)_{18} \cdot 4H_2O$, ein neues Magnesium-Aluminium-Hydroxid-Mineral, Tschermaks Mineral. Petrogr. Mitt. 22 (1975) 79–87.

[56] R. Allmann, H.P. Jepsen, Die Struktur des Hydrotalkits, Neues Jarhb Mineral Monatsh (1969) 544–551.

[57] G. Brown, M.C. Gastuche, Mixed magnesium-aluminium hydroxides II. Structure and structural chemistry of synthetic hydroxycarbonates and related minerals and compounds, Clay Miner. 7 (1967) 193–201.

[58] I.G. Richardson, The importance of proper crystal-chemical and geometrical reasoning demonstrated using layered single and double hydroxides, Acta Crystallogr. B Struct. Crystallogr. Cryst. Chem. 69 (2013) 150–162.

[59] I.G. Richardson, Clarification of possible ordered distributions of trivalent cations in layered double hydroxides and an explanation for the observed variation in the lower solid-solution limit, Acta Crystallogr. B Struct. Crystallogr. Cryst. Chem. 69 (2013) 629–633.

[60] K. Rozov, H. Curtius, A. Neumann, D. Bosbach, Synthesis, characterization and stability properties of Cl-bearing hydrotalcite-pyroaurite solids, Radiochim. Acta 101 (2013) 101–110.

[61] J. Wang, A.G. Kalinichev, J.E. Amonette, R.J. Kirkpatrick, Interlayer structure and dynamics of Cl-bearing hydrotalcite: far infrared spectroscopy and molecular dynamics modeling, Am. Mineral. 88 (2003) 398–409.

[62] H.J. Butt, K. Graf, M. Kappl, Physics and Chemistry of Interfaces, Wiley, New York, 2003.

[63] G. Trefalt, S.H. Behrens, M. Borkovec, Charge regulation in the electrical double layer: ion adsorption and surface interactions, Langmuir 32 (2016) 380–400.

[64] F. Cavani, F. Trifirò, A. Vaccari, Hydrotalcite-type anionic clays: preparation, properties and applications, Catal. Today 11 (1991) 173–301.

[65] V.R.L. Constantino, T.J. Pinnavaia, Basic properties of $Mg_{1-x}^{2+}Al_x^{3+}$ layered double hydroxides intercalated by carbonate, hydroxide, chloride, and sulfate anions, Inorg. Chem. 34 (1995) 883–892.

[66] A. Ookubo, K. Ooi, F. Tani, H. Hayashi, Phase transition of Cl^--intercalated hydrotalcite-like compound during ion exchange with phosphates, Langmuir 10 (1994) 407–411.

[67] W. Meng, F. Li, D.G. Evans, X. Duan, Photocatalytic activity of highly porous zinc ferrite prepared from a zinc-iron(III)-sulfate layered double hydroxide precursor, J. Porous. Mater. 11 (2004) 97–105.

[68] S.-T. Zhang, Y. Dou, J. Zhou, M. Pu, H. Yan, M. Wei, D.G. Evans, X. Duan, DFT-based simulation and experimental validation on the topotactic transformation of MgAl-layered double hydroxides, ChemPhysChem 17 (2016) 2754–2766.

[69] T. Hibino, Y. Yamashita, K. Kosuge, A. Tsunashima, Decarbonation behavior of Mg-Al-CO_3 hydrotalcite-like compounds during heat treatment, Clay Clay Miner. 43 (1995) 427–432.

[70] L. Lv, J. He, M. Wei, D.G. Evans, X. Duan, Uptake of chloride ion from aqueous solution by calcined layered double hydroxides: equilibrium and kinetic studies, Water Res. 40 (2006) 735–743.

[71] M. Balonis, B. Lothenbach, G. Le Saout, F.P. Glasser, Impact of chloride on the

mineralogy of hydrated Portland cement systems, Cem. Concr. Res. 40 (2010) 1009–1022.

[72] A. Mesbah, J.-P. Rapin, M. François, C. Cau-dit-Coumes, F. Frizon, F. Leroux, G. Renaudin, Crystal structures and phase transition of cementitious bi-anionic AFm-(Cl^-, CO_3^{2-}) compounds, J. Am. Ceram. Soc. 94 (2011) 261–268.

[73] R. Rinaldi, M. Sacerdoti, E. Passaglia, Strätlingite: crystal structure, chemistry, and a reexamination of its polytype vertumnite, Eur. J. Mineral. 2 (1990) 841–850.

[74] D.J. Anstice, C.L. Page, M.M. Page, The pore solution phase of carbonated cement pastes, Cem. Concr. Res. 35 (2005) 377–383.

[75] M.U. Okoronkwo, F.P. Glasser, Stability of strätlingite in the CASH system, Mater. Struct. 49 (2016) 4305–4318.

[76] S. Kwan, J. LaRosa, M.W. Grutzeck, ^{29}Si and ^{27}Al MAS NMR study of strätlingite, J. Am. Ceram. Soc. 78 (1995) 1921–1926.

[77] S. Kaufhold, K. Emmerich, R. Dohrmann, A. Steudel, K. Ufer, Comparison of methods for distinguishing sodium carbonate activated from natural sodium bentonites, Appl. Clay Sci. 86 (2013) 23–37.

[78] V. Baroghel-Bouny, X. Wang, M. Thiery, M. Saillio, F. Barberon, Prediction of chloride binding isotherms of cementitious materials by analytical model or numerical inverse analysis, Cem. Concr. Res. 42 (2012) 1207–1224.

[79] F. He, C. Shi, X. Hu, R. Wang, Z. Shi, Q. Li, P. Li, X. An, Calculation of chloride ion concentration in expressed pore solution of cement-based materials exposed to a chloride salt solution, Cem. Concr. Res. 89 (2016) 168–176.

[80] H. Friedmann, O. Amiri, A. Aït-Mokhtar, Physical modeling of the electrical double layer effects on multispecies ions transport in cement-based materials, Cem. Concr. Res. 38 (2008) 1394–1400.